Light-induced properties of Ru-doped $Bi_{12}TiO_{20}$ crystals

2003 J. Opt. A: Pure Appl. Opt. 5 S500

(http://iopscience.iop.org/1464-4258/5/6/017)

INSTITUTE OF PHYSICS PUBLISHING JOURNAL OF OPTICS A: PURE AND APPLIED OPTICS

J. Opt. A: Pure Appl. Opt. **5** (2003) S500–S506 PII: S1464-4258(03)62979-X

Light-induced properties of Ru-doped $Bi_{12}TiO_{20}$ crystals

V Marinova[1,5], S H Lin[1,2], V Sainov[1,3], M Gospodinov[1,4] and K Y Hsu[1]

[1] Institute of Electro-Optical Engineering, National Chiao Tung University, 1001 Ta Hsueh Road, Hsinchu, Taiwan, ROC
[2] Department of Electrophysics, National Chiao Tung University, 1001 Ta Hsueh Road, Hsinchu, Taiwan, ROC
[3] Central Laboratory of Optical Storage and Processing of Information, Bulgarian Academy of Sciences, Sofia, Bulgaria
[4] Institute of Solid State Physics, Bulgarian Academy of Sciences, Sofia, Bulgaria

E-mail: vmarinova@optics.bas.bg and vera@cc.nctu.edu.tw

Received 1 May 2003, accepted for publication 6 October 2003
Published 27 October 2003
Online at stacks.iop.org/JOptA/5/S500

Abstract
Absorption, light-induced absorption, photoconductivity and dark conductivity measurements are performed on $Bi_{12}TiO_{20}$ (BTO) crystals doped with different concentrations of ruthenium. It is found that a higher ruthenium addition shifts the optical absorption to the near-IR spectral region in comparison with non-doped BTO crystals and the absorption changes increase with increasing Ru content. The dark conductivity follows the Arrhenius law with an activation energy of 0.89 eV. From the measured light-induced absorption and nonlinear photoconductivity the participation of a shallow level in the charge transport mechanism in Ru-doped BTO crystals is suggested. Highly Ru-doped BTO samples possess infrared sensitivity and holographic gratings are successfully recorded at 790 and 825 nm, respectively.

Keywords: Photorefractive crystals, doped BTO, light-induced properties, infrared sensitivity

1. Introduction

Photorefractive crystals are attractive materials for many applications. Among them $Bi_{12}TiO_{20}$ (BTO) crystals show some specific photorefractive properties and thus they are of special interest for many applications, such as real-time holography, coherent light amplification, optical phase conjugation, optical information processing, optical interconnection and communications, etc [1–3]. The availability of diode lasers, operating in the near-IR spectral region, stimulated photorefractive crystal optimization and extension of spectral sensitivity into the near-IR by the introduction of intrinsic or extrinsic defects in the crystal structure. Since the defects in the crystal structure are responsible for the photorefractive effect, a detailed knowledge of the light-induced processes and the nature of the photoactive centres is very important.

An effective way to enhance the photorefractive performance is by generating suitable defects in a crystal's structure. The performance of photorefractive crystals depends strongly on impurities, which can act as donors and acceptors for charge carriers. The defects can be modified either by appropriate doping or by nonstoichiometric crystal growth. Moreover BTO crystals can be easily doped and this is a suitable way for the crystal properties to be tailored in a desired direction. The important dopant factors are their concentration, valence state, distribution coefficient, occupied sites symmetry, etc.

The properties of BTO crystals with different doping elements have already been studied [4–7]. However, up to now the influence of Ru on BTO charge-transport properties is still under investigation. It was found that low Ru concentration

[5] On leave from: Central Laboratory of Optical Storage and Processing of Information, Bulgarian Academy of Sciences, Sofia, Bulgaria.

could enhance the optical and photorefractive properties of BTO crystals at He–Ne laser wavelengths [8]. Furthermore, it was reported that Ru addition shows perspective features in $Sr_{0.61}Ba_{0.39}Nb_2O_6$ crystals [9].

The aim of our investigation is to determine the influence of Ru doping on the light-induced properties of BTO crystals in an attempt to improve the photorefractive properties in the near-IR region.

2. Experiment

2.1. Crystals

BTO single crystals doped with two different ruthenium concentrations were grown in a Czochralski apparatus using the top seeded solution growth method. The purity of the starting products Bi_2O_3 and TiO_2 was 99.999% and their weight proportion was 11:1. Ruthenium was introduced into the melt solution in the form of RuO_2. The concentrations of Ru in the grown crystals determined by atomic absorption spectroscopy were 1×10^{18} and 1×10^{19} cm^{-3} and these crystals were called hereinafter BTO:Ru18 and BTO:Ru19, respectively.

2.2. Absorption and light-induced absorption

Transmission spectra were measured on double polished plates in the wavelength range 400–850 nm using a Cary 5I spectrophotometer. Reflection spectra were measured on plates with one polished and one ground side in the visible spectrum using a Perkin-Elmer 330 spectrophotometer with special references for calibration at 488, 514.5, 576, 633 and 672 nm. The absorption coefficient α (cm^{-1}) was calculated by taking into account the crystal's transmission, reflection and thickness.

For the light-induced absorption measurements, crystals were illuminated with a 'pump' light with a fixed wavelength of $\lambda = 532$ nm (using a Verdi solid-state laser). Simultaneously a weak 'probe' light emitted by a 240 W QTH lamp of a grating monochromator (Oriel MS 257) illuminated the samples. The probe beam intensity I_{probe} was kept small (several μW) to avoid any additional absorption changes. The probe beam transmitted through the crystal was collected by a computer-controlled photomultiplier tube (PMT). A holographic notch filter for 532 nm was placed in front of the PMT in order to eliminate the influence of the pump beam scattering light. The complete set-up for light-induced absorption and photoconductivity measurements is shown in figure 1.

The light-induced absorption change α_{li} (cm^{-1}) was calculated from the change of the transmitted probe light intensity, using the following formula [10]:

$$\alpha_{\text{li}} = \frac{1}{d} \ln\left[\frac{I_{\text{pump off}}}{I_{\text{pump on}}}\right] \tag{1}$$

where d is the crystal thickness and $I_{\text{pump on}}$ and $I_{\text{pump off}}$ are the values of the intensities of the transmitted probe light when the pump light is switched on and off, respectively.

2.3. Dark conductivity and photoconductivity

Silver surface electrodes separated by a 0.2–0.5 mm gap were made for measurements of the dark conductivity and photoconductivity characteristics of the samples investigated. The dark conductivity measurements were carried out using a Keithley 6487 pico-ammeter/voltage supply. For temperature measurements we used a custom-made holder with cartridge heaters. The crystal temperature was measured by a Pt thermocouple, mounted just above the sample. The temperature was controlled to within an error of ± 1 K. For photoconductivity measurements a QTH and ARC lamp sources connected with the same grating monochromator was used.

During the study of photocurrent dependence on wavelength we made a reverse scan, e.g. scanning always started from 800 to 400 nm. Also, we waited several minutes after any change of light or intensity before the measurement value was taken in order for the sample to reach an equilibrium state.

2.4. Near-IR holographic recording in highly Ru-doped BTO

Holographic recording was performed using a two-beam coupling technique at 790 and 825 nm wavelengths. During the experiments an external electric field of $E_0 = 2$ kV cm^{-1} was applied. Only a highly Ru-doped sample shows photorefractive properties at these wavelengths. It was not possible to record gratings for non-doped and BTO:Ru18. Highly Ru-doped BTO with dimensions $6 \times 6 \times 5$ mm^3, whose edges are oriented with respect to the crystallographic [110], [1$\bar{1}$0] and [001] directions, was used for our experiments. A diode laser source input was split into two interfering beams I_R and I_S of equal intensities. The writing angle θ was 34° and the grating vector was perpendicular to the [001] direction. During writing, one of the recording beams was blocked for about 0.05 s and another beam was used to monitor the grating build-up and to measure the diffraction efficiency η. Here η was defined as $I_d/(I_d + I_t)$, where I_d and I_t were the diffracted and transmitted intensities of the readout beam, respectively. Note that recorded gratings were readout by one of the recording beams with the same intensity used during the writing process.

3. Results and discussion

3.1. Absorption and light-induced absorption

Figure 2 shows the absorption coefficient dependence on photon energy for lower and higher concentrations of Ru in comparison with non-doped BTO. As is shown, a low concentration of ruthenium do not change the absorption shoulder of BTO. However, higher ruthenium addition (BTO:Ru19) significantly shifts the optical absorption to the near-IR spectral region with an absorption shoulder appearing at 1.8 eV. Obviously the absorption changes increase with increasing Ru content. A typical well-defined broad absorption shoulder is observed in BTO:Ru18 and non-doped BTO, extending from the band edge (3.2 eV) up to 2.3 eV. According to Oberschmid [11] this absorption shoulder is due to the contribution of an intrinsic antisite defect (Bi^{3+} + h) formed by occupation of a tetrahedrally coordinated Ti^{4+} site by a

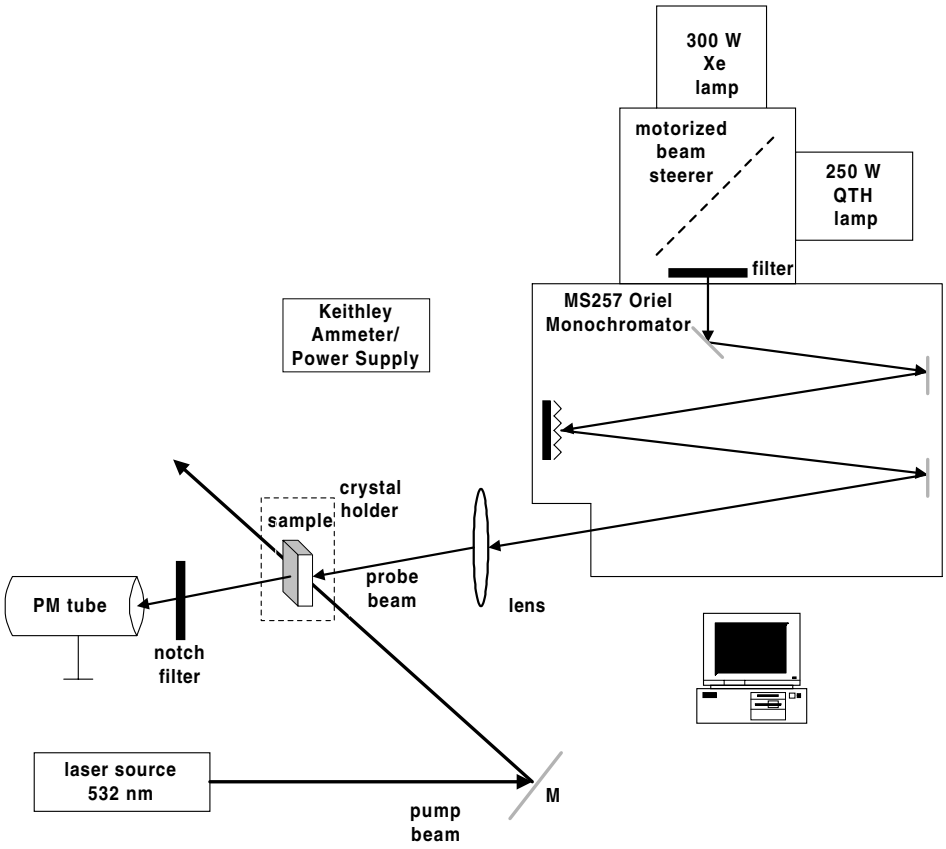

Figure 1. Experimental set-up for light-induced absorption and photoconductivity measurements.

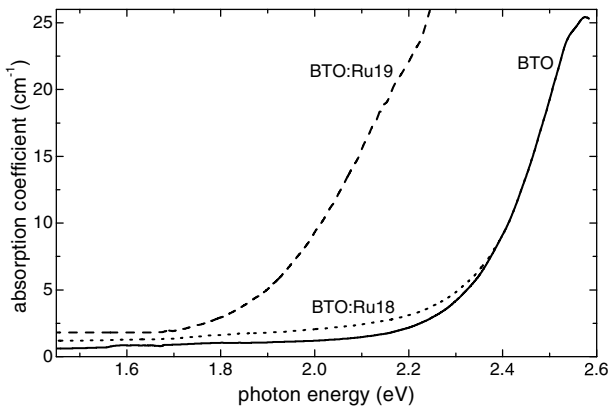

Figure 2. Absorption coefficient dependence on photon energy of BTO crystals doped with different concentrations of Ru.

Bi^{3+}, coupled with a hole, mainly localized at the oxygen neighbours.

Illumination of samples with a pump light generates light-induced absorption changes. Figure 3 shows the light-induced absorption dependence on the probe photon energy (continuous monochromatic scanning) under illumination with a pump light (532 nm, 0.6 W cm^{-2} intensity) for all samples investigated. Experimental results shown in figure 3 show that, after illumination with a pump light, electron redistribution from the deep to the shallow levels occurs. As a result absorption is changed, $\alpha_{\rm li} > 0$, because the photon absorption cross section S becomes different for the deep and shallow traps, leading to $S_{\rm S} > S_{\rm D}$, where $S_{\rm S}$ and $S_{\rm D}$ are excitation cross sections of the shallow and deep donor, respectively. Since the absorption cross section generally varies with the probe photon energy, light-induced absorption also changes with the probe wavelength. As is seen samples doped with low Ru concentration possess a little higher light-induced absorption than un-doped BTO crystals and the maximum value reached is $\alpha_{\rm li} = 0.36\,{\rm cm}^{-1}$. For lower Ru concentrations light-induced transparency appears when the probe photon energy is above 1.8 eV (around 700 nm). However, even at the same pump intensity, the light-induced absorption for highly Ru-doped BTO is much higher for the whole visible spectral range. This indicates that the concentration of shallow traps increases with increasing Ru content.

The dynamics of light-induced absorption was measured during green pump light illumination and after the pump light is switched off. Figure 4(a) shows an example of a typical build-up process of light-induced absorption (after the pump light is switched on at time $t = 0$) for a BTO:Ru19 sample. The probe wavelength was selected to be 790 nm (1.6 eV). The focus of these investigations are mainly concentrated on BTO:Ru19 since this shows promising behaviour in the near-IR region. A decrease of the probe beam intensity was observed after the pump beam was switched on. The light-induced absorption change takes place for several seconds, suggesting that shallow traps are populated during pump light illumination.

The dark-decay dynamics of the light-induced absorption immediately after the pump light is switched off is shown in figure 4(b). Usually the dark decay is associated with the loss

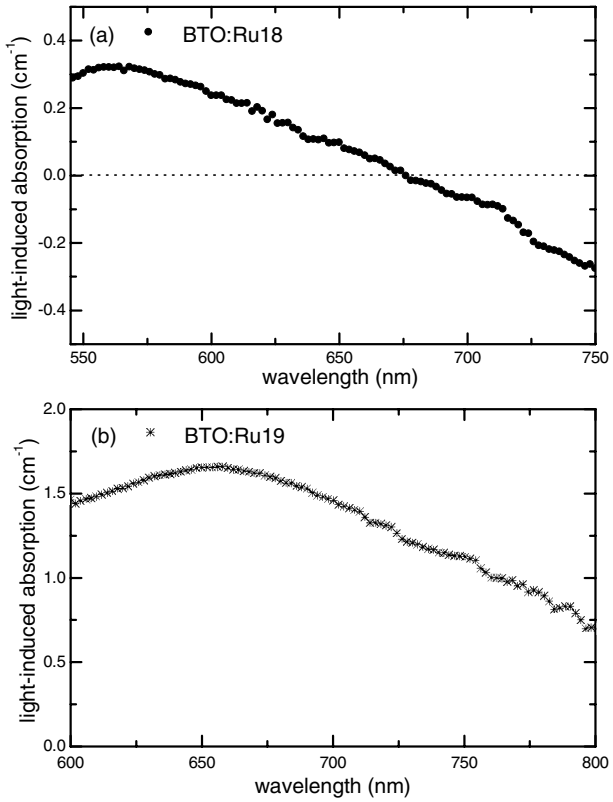

Figure 3. Spectra of light-induced absorption changes versus probe photon energy. The pump light is $\lambda = 532$ nm with intensity $I = 0.6$ W cm^{-2}.

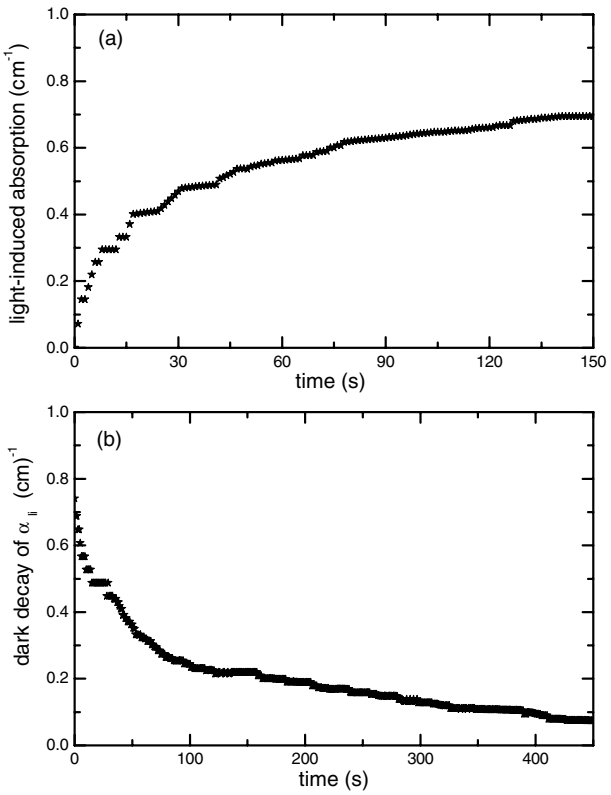

Figure 4. Build-up (a) and dark decay (b) of light-induced absorption for BTO:Ru19. The pump light is $\lambda = 532$ nm with intensity $I = 0.3$ W cm^{-2} and the probe light is $\lambda = 790$ nm.

of the population of shallow traps by thermal ionization. As can be seen the dark relaxation could be described as a two-step process, the first decay process being much faster than the second one. From the preliminary experimental results it is easy to separate out two time constants—the first process occurs within a few seconds while the second one needs more time. The dark decay indicates that the relaxation time for the light-induced absorption may be as long as several minutes or hours. This demonstrates that secondary shallow traps are located in the Ru-doped BTO structure.

Experimental results show that Ru-doped BTO crystals exhibit light-induced absorption changes, suggesting the existence of both deep and shallow traps. The light-induced absorption changes due to the filling of shallow traps are usually described by a two-centre model or three-valence model [10, 12–14]. Due to the results shown in figure 4, we assume the presence of one deep photorefractive level N_1 and two shallow centres N_{2a} and N_{2b}. The level N_{2a} is close to the conduction band and the level N_{2b} is between N_1 and N_{2a} due to the two time constants during the dark-decay process. Furthermore, preliminary results show that light-induced phenomena depend on preliminary treatment of the sample and thermal annealing could strongly influence the shallow trap concentration.

All the above-presented experimental results show that more shallow centres appear in Ru-doped BTO crystals. The absorption, light-induced absorption and effective trap density increase with increasing Ru concentration.

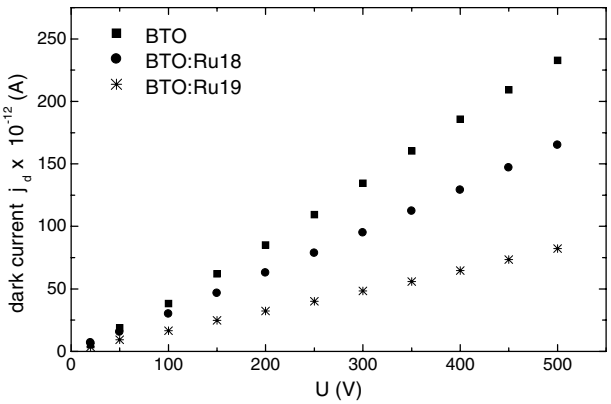

Figure 5. I–V characteristics under dark conditions at room temperature for all samples investigated.

3.2. Ohmic behaviour

Current–voltage characteristics for all crystals investigated in dark conditions at room temperature are shown in figure 5. The dark conductivity σ_d decreases with increasing Ru doping from 7.6×10^{-15} Ω^{-1} cm^{-1} (for nominally pure BTO) to 2.4×10^{-15} Ω^{-1} cm^{-1} (for BTO:Ru19). A low dark conductivity is very important for holographic recording. The values of dark conductivity are summarized in table 1.

The dark conductivity σ_d temperature dependence is shown in figure 6. As can be observed, the conductivity increases with temperature. The activation energy values were derived from the plots in figure 6, which follow the Arrhenius

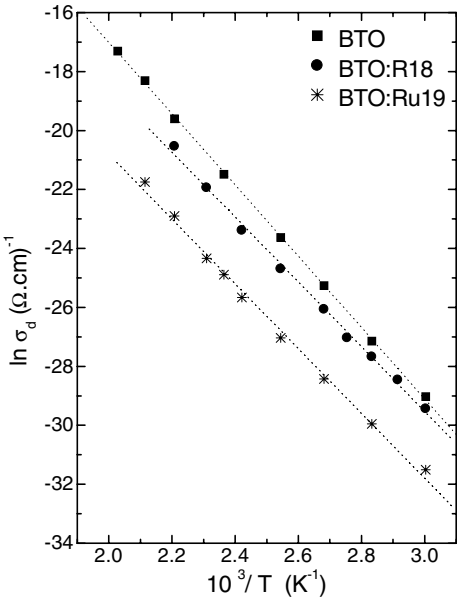

Figure 6. Arrhenius plot of the dark conductivity σ_d. The symbols are measured data, while the dotted line is a linear fit yielding the activation energy E_a.

Table 1. Dark conductivity σ_d and activation energy (E_a) values of Ru-doped BTO crystals.

Sample	σ_d ($\times 10^{-15}$ Ω^{-1} cm^{-1})	E_a (eV)
BTO	7.6	1.06 ± 0.05
BTO:Ru18	5.2	0.89 ± 0.05
BTO:Ru19	2.4	0.89 ± 0.05

law:

$$\sigma = \sigma_0 \exp(-E_a/k_B T) \qquad (2)$$

where σ_0 is a pre-exponential factor, E_a is the activation energy for conduction, T is the absolute temperature and k_B is Boltzmann's constant. The calculated data for activation energies are summarized in table 1. The value obtained of 1.06 eV for non-doped BTO is similar to the data reported by other authors ($E_a = 0.99$ eV) [15, 16] and coincides very well with $E_a = 1.06$ eV determined by Mersch *et al* [4]. Ru doping creates a new centre in the BTO inter-band structure with a thermal activation energy of 0.89 eV.

The photocurrent density j_i was measured in an external electric field E_o (V cm^{-1}) depending on the wavelength and on different light intensities I. The photocurrent was detected by measuring the dark current j_d and the current under light illumination j_i. Subtracting j_d from j_i yields the photocurrent j_{ph} ($j_{ph} = j_i - j_d$). From the photocurrent density j_{ph} we calculated the photoconductivity $\sigma_{ph} = j_{ph}/E_0$. The photoconductivity determines the speed of the build-up and decay of the refractive index change during holographic recording and depends on the ratio of filled to empty traps. The photocurrent density spectral dependence of BTO:Ru18 and BTO:Ru19 is shown in figures 7 and 8, respectively. As can be seen the illumination caused a large increase in conductivity. It is supposed that decreasing the number of recombination centres, and as a result increasing the photocarriers' lifetime, leads to the increase in photoconductivity. The photocurrent density behaviour of the crystal sample doped with a lower

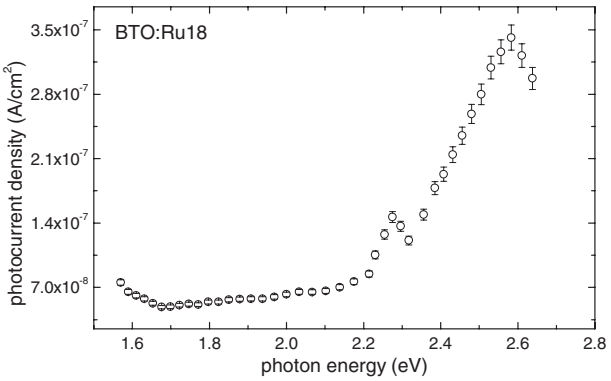

Figure 7. Spectral dependence of photocurrent density on wavelengths for a BTO:Ru18 crystal.

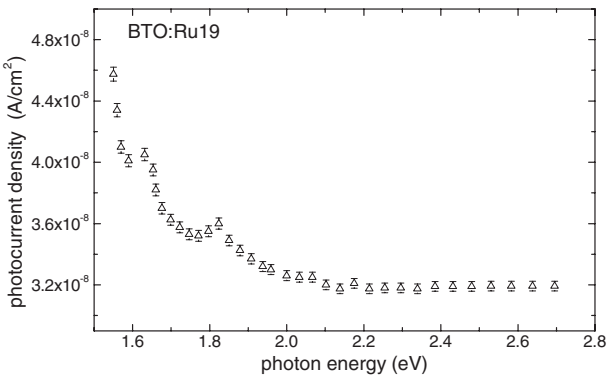

Figure 8. Spectral dependence of photocurrent density on wavelengths for a BTO:Ru19 crystal.

Ru concentration is very similar to that of the non-doped BTO spectrum. However, the carrier density becomes higher with Ru addition. The spectral distribution of the photocurrent density values in figure 7 shows peaks at 2.6 and 2.3 eV, probably due to the donor levels in the bandgap. Furthermore, these peak positions indicate that in BTO:Ru18 the nature of the absorption centres, responsible for photo-induced phenomena, is the same as in BTO. As can be seen in figure 8 for higher Ru concentrations photocurrent spectra show a peak at 1.8 eV, which corresponds to the extrinsic absorption in figure 2. It is supposed that the nature of the centre responsible for the extrinsic absorption and photoconductivity is the same as in BTO:Ru19. An additional peak was detected at around 1.6 eV, which we could not see in the absorption spectrum. However, our preliminary holographic testing of BTO:Ru19 at 790 nm shows interesting photorefractive properties. Furthermore, a highly Ru-doped sample shows a promising photocurrent increase in the near-IR region.

Figures 9(a) and (b) show saturation effects of the photoconductivity σ_{ph} dependence on light intensity for a BTO:Ru18 crystal using light sources of 532 and 633 nm, respectively. The photoconductivity increases nonlinearly with light intensity. A similar nonlinear dependence shows BTO:Ru19 at a wavelength of 790 nm. The light-induced absorption changes and nonlinear dependence of photoconductivity on light intensity indicate that deep and shallow photoactive levels contribute to the charge transport in Ru-doped BTO.

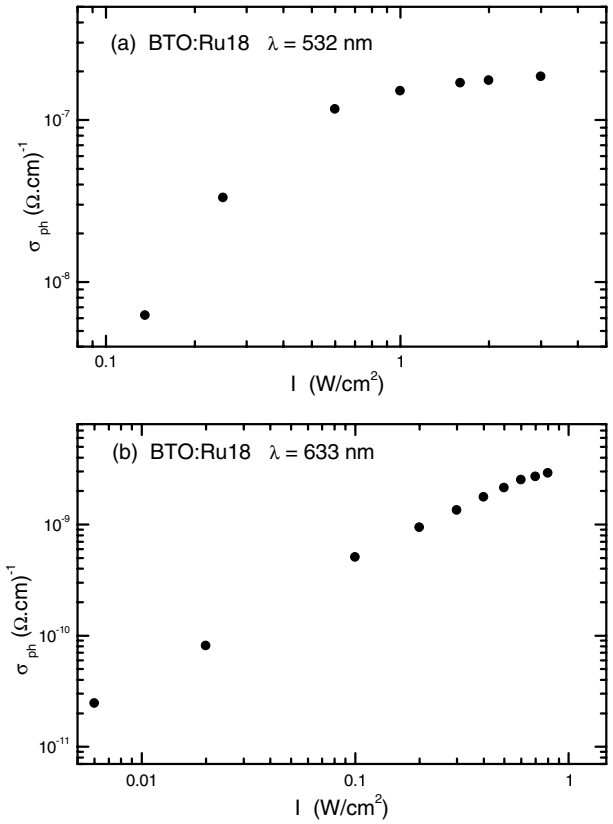

Figure 9. Photoconductivity σ_{ph} dependence on light intensity for a BTO:Ru18 crystal at: (a) 532 nm and (b) 633 nm.

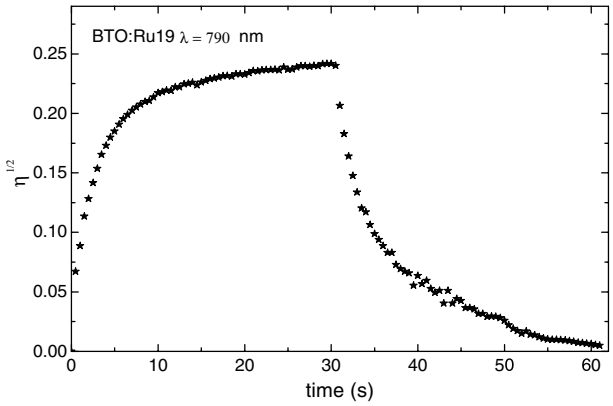

Figure 10. Time dependence of the square root of the diffraction efficiency during holographic writing and reading at 790 nm in a highly Ru-doped BTO crystal.

3.3. Near-IR holographic recording

Figure 10 shows a typical grating build-up dynamics and readout process in highly Ru-doped BTO at 790 nm. The writing kinetics shows fast growth, on a timescale of a few seconds. A holographic grating, recorded at 825 nm, shows a similar behaviour. However, the grating recorded at 790 nm possesses a higher diffraction efficiency and faster response time τ_r ($\tau_r = 3.8$ s at 790 nm and $\tau_r = 5$ s at 825 nm).

The refractive index modulation was calculated from the experimental diffraction efficiencies using Kogelnik's formula [17]:

$$\eta = \exp\left(-\frac{\alpha d}{\cos\theta}\right)\sin^2\left(\frac{\pi \Delta n d}{\lambda \cos\theta}\right) \tag{3}$$

where α is the absorption coefficient, d is the crystal thickness, λ is the wavelength of light in a vacuum and θ is the angle between the recording beams inside the crystal. During the holographic experiments the maximum induced refractive index modulation for BTO:Ru19 is $\Delta n = 1 \times 10^{-5}$ at $\lambda =$ 790 nm and $\Delta n = 4 \times 10^{-6}$ at $\lambda = 825$ nm, respectively.

It is well known that BTO crystals have a complex structure that allows for a number of charge trapping sites. Usually, the deep level is related to the intrinsic defects due to the Ti^{4+} or replaced by (Bi^{3+} + h) vacancies in tetrahedral positions [11]. The dark conductivity in silenites is assumed to be a p-type due to an acceptor centre formed by occupation of a tetrahedrally coordinated Ti^{4+} site by a Bi^{3+} coupled with a hole h (Bi^{3+} + h). However, the conductivity under the action of light is known to be due to electrons [3]. In the case of Ru doping the bandgap becomes more complicated due to the assumption, based on magnetic circular dichroism (MCD) studies [18], that Ru ions can exist simultaneously in three different valence states: Ru^{3+}, Ru^{4+} and Ru^{5+}. It should be noted that in our highly doped BTO crystal Ru is present at a large concentration and it will probably have a substantial contribution to the photorefractive properties in the near-IR region. Furthermore, the distribution coefficient of Ru in the BTO structure is high, i.e. the ruthenium concentration in the melt and in the crystal is nearly the same.

Usually, such impurities like Ru that can occur in three valence states are undesirable, since it is difficult to control the light-induced behaviour. On the other hand, large concentrations of shallow levels should be useful for IR sensitization. We supposed that Ru doping generates new trap centres in the BTO structure; however, further experiments are underway in order to determine the ideal concentration.

4. Conclusions

High Ru addition to BTO crystals shifts the optical absorption to the near-IR spectral region and creates an absorption shoulder at 1.8 eV. Absorption, light-induced absorption and effective trap density increase with increasing Ru concentration. The dark conductivity follows the Arrhenius law with an activation energy of 0.89 eV. Holographic gratings at 790 and 825 nm are recorded with refractive index modulation 1×10^{-5} and 4×10^{-6}, respectively. Light-induced absorption changes and the nonlinear dependence of photoconductivity on light intensity indicate that at least two photoactive levels contribute to the charge transport in Ru-doped BTO.

Acknowledgments

This work was supported by contract 89-E-FA06-1-4 by the Ministry of Education, Taiwan, Republic of China and the Taiwan–Bulgarian collaboration program agreement NSC91-2911-I-009-010. Ru-doped BTO crystals were grown in the Crystal Growth Laboratory, Institute of Solid State Physics, Bulgarian Academy of Science.

References

[1] Coufal H J, Psaltis D and Sincerbox G T (ed) 2000 *Holographic Data Storage* (Berlin: Springer)

[2] Gunter P and Huignard J P (ed) 1988 *Photorefractive Materials and their Applications* vol 1 (Berlin: Springer)

[3] Arizmendi L, Cabrera J and Agullo-Lopez F 1992 Materials properties and photorefractive behavior of BSO family crystals *Int. J. Optoelectron.* **7** 149–80

[4] Mersch F, Buse K, Sauf W, Hesse H and Kratzig E 1993 Growth and characterization on undoped and doped $Bi_{12}TiO_{20}$ crystals *Phys. Status Solidi* a **140** 273–81

[5] Riehemann S, Dirksen D and Von Bally G 1995 Non-exponential build-up and decay of holographic grating in $Bi_{12}Ti_{0.76}V_{0.24}O_{20}$ crystals *Solid State Commun.* **95** 529–32

[6] Coya C, Zaldo Z, Volkov V V, Egorisheva A V, Polgar K and Peter A 1996 Gallium-induced inhibition of the photorefractive properties of silenite crystals *J. Opt. Soc. Am.* B **13** 908–15

[7] Mosquera L, de Olivera J, Frejlich J, Hernandes A C, Lanfredi S and Carvalho J F 2001 Dark conductivity, photoconductivity and light-induced absorption in photorefractive silenite crystals *J. Appl. Phys.* **90** 2635–41

[8] Marinova V, Hsieh M L, Lin S H and Hsu K Y 2002 Effect of ruthenium doping on the optical and photorefractive properties of $Bi_{12}TiO_{20}$ single crystals *Opt. Commun.* **203** 377–84

[9] Fujimura R, Kubota E, Matoba O, Shimura T and Kuroda K 2002 Photorefractive and photochromic properties of Ru-doped $Sr_{0.61}Ba_{0.39}Nb_2O_6$ crystals *Opt. Commun.* **213** 373–8

[10] Buse K 1997 Light-induced charge transport properties in photorefractive crystals I. Models and experimental methods *Appl. Phys.* B **64** 273–91

[11] Oberschmid R 1985 Absorption centers of $Bi_{12}GeO_{20}$ and $Bi_{12}SiO_{20}$ crystals *Phys. Status Solidi* a **89** 263–70

[12] Brost G A, Motes R A and Rotge J R 1988 Intensity dependent absorption and photorefractive effects in barium titanate *J. Opt. Soc. Am.* B **5** 1879–85

[13] Buse K 1997 Light-induced charge transport properties in photorefractive crystals II. Materials *Appl. Phys.* B **64** 391–407

[14] Buse K and Kratzig E 1995 Three-valence charge transport model for explanation of the photorefractive effect *Appl. Phys.* B **61** 27–32

[15] Riehemann S, Rickermann F, Volkov V, Egorysheva A and Von Bally G 1997 Optical and photorefractive characterization of BTO crystals doped with Cd, Ca, Ga and V *Int. J. Nonlinear Opt. Phys. Mater.* **6** 235–49

[16] Lanfredi S, Carvalho P and Hernandes A C 2000 Electric and dielectric properties of $Bi_{12}TiO_{20}$ single crystal *J. Appl. Phys.* **88** 283–7

[17] Kogelnik H 1969 Coupled wave theory for thick hologram gratings *Bell Syst. Tech. J.* **48** 2909–47

[18] Rjeily H B, Ramaz F, Petrova D, Gospodinov M and Briat B 1997 Absorption and MCD study of photochromism in $Bi_{12}SiO_{20}$ doped with 4d or 5d transition metal ions *Proc. SPIE* **3178** 169–72